Improving the performance of alkali-activated slag mortar with electro/chemically treated carbon fiber textile

Downloaded from: https://research.chalmers.se, 2026-04-04 03:49 UTC

Citation for the original published paper (version of record):
Huang, L., Tang, L., Bachinger, A. et al (2023). Improving the performance of alkali-activated slag mortar with electro/chemically treated
carbon fiber textile. Journal of Cleaner Production, 418.
http://dx.doi.org/10.1016/j.jclepro.2023.138214

N.B. When citing this work, cite the original published paper.

research.chalmers.se offers the possibility of retrieving research publications produced at Chalmers University of Technology. It covers all kind of research output: articles, dissertations, conference papers, reports etc. since 2004. research.chalmers.se is administrated and maintained by Chalmers Library

(article starts on next page)

Journal of Cleaner Production 418 (2023) 138214

Contents lists available at ScienceDirect

Journal of Cleaner Production

journal homepage: www.elsevier.com/locate/jclepro

Improving the performance of alkali-activated slag mortar with electro/chemically treated carbon fiber textile

Liming Huang [a,b,*], Luping Tang [a,**], Angelika Bachinger [c], Yongqiang Li [d], Zhenghong Yang [b]

[a] Department of Architecture and Civil Engineering, Chalmers University of Technology, 41296, Gothenburg, Sweden
[b] Key Laboratory of Advanced Civil Engineering Materials Ministry of Education, Tongji University, Shanghai, 201804, PR China
[c] Department of Polymers, Fibers and Composites, RISE Research Institutes of Sweden, 43122, Mölndal, Sweden
[d] College of Civil and Transportation Engineering, Shenzhen University, Shenzhen, 518060, Guangdong, PR China

ARTICLE INFO

Handling Editor: Zhen Leng

Keywords:
Carbon fiber textile
Alkali-activated slag
Bonding strength
Electroplating treatment

ABSTRACT

Alkali-activated slag is a widely used low-carbon binder. Incorporation of textile can mitigate the brittle weakness of alkali-activated composites. The bonding between fibers and matrix is critical for the performance of textile reinforced mortar. This paper is focused on the effect of different treatment methods on the bonding properties of carbon fiber in alkali-activated slag. The interfacial shear strength of fiber bundles in matrix was determined by the pull-out test. The flexural strength of the reinforced mortar was evaluated by a repeated bending. A scanning electron microscopy test was performed to characterize the interfacial properties of the fiber bundles. The results show that the interfacial shear strength of carbon fibers in matrix is improved by the electroplating with calcium silica slurry (CSS), impregnation in different solutions, and plasma treatments. An electroplating in CSS has the best improvement in the bonding strength with an increase by 620%. The CSS treatment increases the maximum flexural strength of CFT reinforced mortar with 22.5% and 30% at 7 and 28 d respectively, and it significantly inhibits the crack growth under the cyclic loading. This effect becomes more significant after a longer curing age. The electroplating treatment eliminates the cracks in the interface of fiber yarns. Slag reacts with the plated portlandite to strengthen the bonding between mortar and fiber bundles, so it has a better inhibiting effect on the crack growth after a longer curing.

1. Introduction

The alkali-activated binders have a much lower carbon footprint than Portlandite cement during the production process, so the development of these binders has been recognized as a promising way to reduce the carbon emissions in the construction sector (Shi et al., 2019). Moreover, the alkali-activated concretes have a superior fire and corrosion resistance, higher durability, and similar compressive strength compared with Portland cement concrete. Therefore, the commercial-scale application of alkali-activated binders in buildings and infrastructure is proceeding rapidly in many nations (Provis et al., 2015).

However, Alkali-activated concrete typically exhibits a lower flexural strength compared to Portland cement concrete with similar compressive strength, making brittle failure a major concern during its service life (Ding et al., 2016). The incorporation of fibers is an effective and popular way to overcome the brittle characteristics of the alkali-activated slag (AAS) concrete. Many kinds of fibers were used to reinforce the AAS, such as polypropylene fiber (Behfarnia and Rostami, 2017; Choi et al., 2021), steel fiber (Bernal et al., 2010; Aydın and Baradan, 2013; Karunanithi, 2017; Niş et al., 2021), carbon fiber (CF) (Vilaplana et al., 2016; Cui et al., 2018), basalt fiber (BF) (Zhou et al., 2022), and glass fiber (Yurt, 2020). These fibers in general increase the flexural strength of the alkali-activated composites with a possible maximum factor of 5 times, which depends on the types, dimension, the shape and dosage of fibers (Ranjbar and Zhang, 2020). The fibers with a higher Young's modulus (such as steel and carbon fibers) can better sustain the internal stresses to avoid some local fracture induced by concentrations of stress (Amran et al., 2022).

Carbon fibers have a very high specific strength and lightest weight among all reinforcing fibers (Chung, 2016; Ranjbar and Zhang, 2020). They present an outstanding tensile strength and modulus, a good

* Corresponding author. Department of Architecture and Civil Engineering, Chalmers University of Technology, 41296, Gothenburg, Sweden.
** Corresponding author. Department of Architecture and Civil Engineering, Chalmers University of Technology, 41296, Gothenburg, Sweden.
E-mail addresses: limingh@chalmers.se (L. Huang), tang.luping@chalmers.se (L. Tang).

https://doi.org/10.1016/j.jclepro.2023.138214
Received 19 December 2022; Received in revised form 22 June 2023; Accepted 20 July 2023
Available online 21 July 2023
0959-6526/© 2023 The Authors. Published by Elsevier Ltd. This is an open access article under the CC BY license (http://creativecommons.org/licenses/by/4.0/).

Table 1
The chemical composition of binders.

Chemical composition (%)	CaO	SiO_2	Al_2O_3	Fe_2O_3	MgO	Na_2O	K_2O	MnO	TiO_2	LOI
Slag	40.62	38.71	10.46	0.33	7.58	0.54	0.35	0.21	0.37	0.83
Cement	61.81	19.32	7.90	2.69	0.81	0.11	1.02	0.06	0.23	2.96

chemical stability and thermal stability. Therefore, carbon fibers are commonly used to reinforce the alkali-activated concrete. Vilaplana et al. (2016) reported that the inclusion of 1% CF in AAS had a weak effect on the compressive strength but it induced a significant increase in the bending strength by about 3 times at 60 d. They also found that the incorporation of CF reduced the drying shrinkage. Cui et al. (2018) incorporated 1% CF into ordinary Portland cement and AAS concrete. Their results showed that the flexural strength of both Portland cement and AAS concrete was significantly increased by CF, and this effect was more significant in AAS concrete than Portland cement concrete.

The textiles consist of several yarns fabricated with plenty of filaments. The use of carbon fiber textile (CFT) has a higher effectiveness in comparison with the dispersed short fibers (Brameshuber, 2006). The textile can provide a higher tensile strength, lower self-weight and greater resistance to corrosion compared to traditional steel reinforcement (Liu et al., 2020). Moreover, the textiles are very flexible, and they can provide multi-dimensional enhancement in the ultrahigh performance concrete (Meng et al., 2018). The performance of both the short fiber reinforced (Wu et al., 2018) and textile fiber reinforced concretes (Carozzi and Poggi, 2015; Raoof et al., 2016) is largely affected by the bonding strength between fibers and concrete matrix.

Researchers have employed many approaches to improve the bonding strength between fibers and matrix, such as mechanical modification (Singh et al., 2004), chemical treatment (López-Buendía et al., 2013; Park et al., 2008), and plasma modification (Trejbal et al., 2016). The main purpose of these treatments is to increase the surface roughness or to activate polar groups on the surface of the fibers. Some investigations tried to coat the active SiO_2 on fiber surface so that it can react with portlandite in the matrix to increase the bonding strength. Lu et al. (2018) proposed a method to improve the bonding strength between CF and cement matrix by coating with nano-SiO_2. They designed complex procedures to induce the condensation and polymerization of the tetraethyl orthosilicate by the chemical reaction in alkaline solutions. Li et al. (2020) applied electrophoretic deposition method to coat nano-silica on the CF thus improving its bonding to cementitious matrices. It should be noted that the performance of chemically treated fibers varies in different binders (Li et al., 2002; Nematollahi et al., 2017). The alkali-activated binders commonly have less CaO but more SiO_2 and Al_2O_3 in the chemical compositions compared with Portland cement. A coating of Ca-rich layer in the CFT would have a good improvement in the bonding strength between textile and alkali-activated binder, because it has the potential to react with the SiO_2 or Al_2O_3 in binders.

To our best knowledge, there is no such research on how to coat a Ca-rich layer on the carbon fibers as well as its application in the alkali-activated slag mortar. Herein, we proposed a novel method to coat a Ca-rich layer on the CFT by electroplating. The effect of this coating method has been compared with other impregnation treatments in different kinds of slurries. The interfacial shear strength between different fiber yarns and matrix was measured by the pull-out test. The flexural strength and crack growth of the electroplated CFT reinforced AAS mortar was compared with that of the commercial CFT reinforced mortar. A measurement by the scanning electron microscopy under backscatter mode (BSEM) was performed to analyze the interfacial properties between the AAS matrix and CFT. The mechanism of improving the bonding performance between electroplated CFT and matrix was discussed.

2. Materials and methods

2.1. Materials

The main binder is the ground granulated blast-furnace slag (Merit 5000) from Merox AB. The mortar was also mixed with a small amount

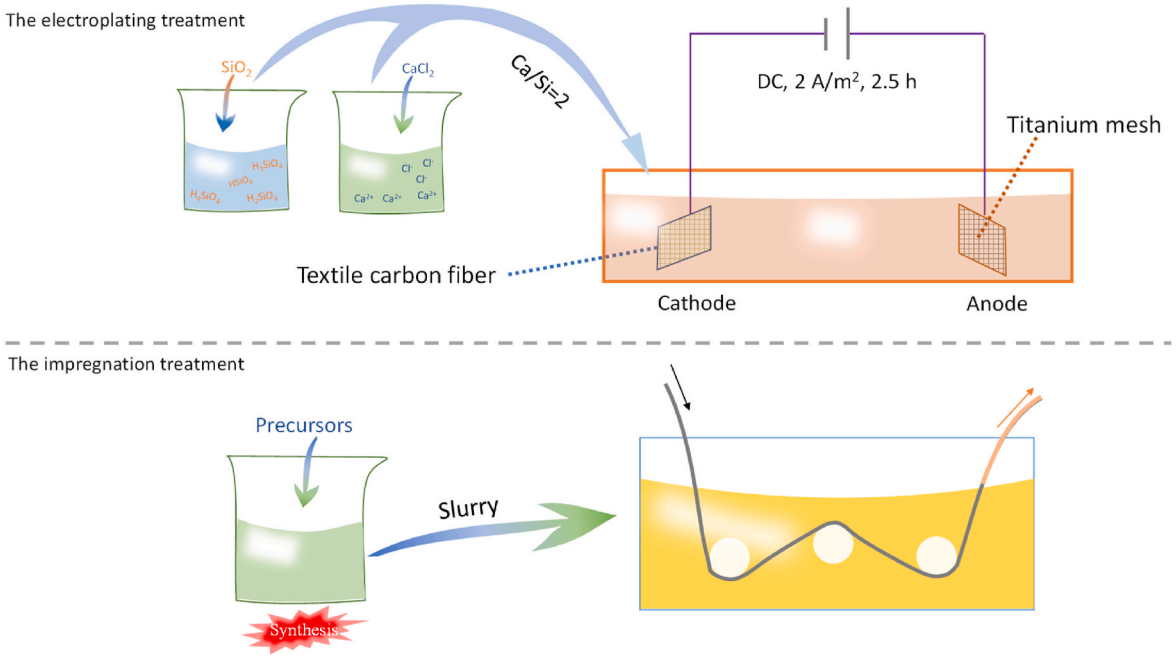

Fig. 1. Different methods for the treatment of CFT.

Table 2
Mix of the suspension for electroplating of CFT.

Concentration of the materials (g/L)		Mixed with volume ratio	CaO/SiO_2 (mol)	Viscosity at 100 rpm (mPa·s)
$CaCl_2$	SiO_2			
363	100	1:1	2.0	130–140

of Swedish Portland-limestone cement (CEM II/A-LL 42.5 R). The chemical compositions of slag and cement are shown in Table 1. Water glass (sodium silicate, $Na_2O{\cdot}xSiO_2$) was supplied by Sibelco Nordic with the initial molar ratio (Mr) of 3.34. Sodium hydroxide (NaOH) pellets (pure, Thermo Scientific® or EMPLURA®) was added to the water glass to adjust the molar ratio to a desired value. Gypsum and sand with standard grades were purchased in a local market. Colloidal silica (Levasil CB8) was supplied by AkzoNobel. The other materials were purchased from Sigma Aldrich, including calcium chloride (industrial grade), hydrochloric acid (37%, EMSURE®, reagent grade) and kaolin (particle size < 2 μm), Tetraethyl orthosilicate (TEOS), 3-(Trimethoxysilyl)propyl methacrylate (MEMO) and Vinyltrimethoxysilane (VTMOS).

The untreated carbon fiber textile (mesh) was purchased from Nanjing Haituo Composite Materials Co. Ltd., with the mesh size of 10 mm (including warp 4 mm with 12k fibers and space 6 mm) by 8 mm (including weft 3 mm with 6k fibers and space 5 mm). The other commercial fiber textiles include the styrene-butadiene rubber (SBR) impregnated carbon fiber textile (SITgrid017 by V. Fraas GmbH, Germany) and the basalt fiber textile (BFT) (US GRD 25–100 from US Basalt). Some more detailed information of binders and fibers was recorded in a previous report (Bachinger et al., 2021b).

2.2. Preparation of the samples

2.2.1. The electroplating treatment

A technique developed by (Tang et al., 2020) was employed for electroplating treatment of carbon fibers in this study. Colloidal silica suspension (51% solid content) was diluted with the deionized water to obtain an aqueous solution with a SiO_2 concentration of 100 g/L. The other solution was prepared by dissolving the $CaCl_2$ into the deionized water to a $CaCl_2$ concentration of 363 g/L. The two different solutions were mixed with a volume ration of 1:1 in a container with stirring to produce a calcium silica slurry (CSS) as the electrolyte (see the upper part in Fig. 1). Table 2 shows an example of the mix proportion of electrolyte, and the viscosity of the slurry is 130–140 mPa s (measured by the viscometer, Anton Paar Visco QC 300–H, at a speed of 100 r/min).

The CFT was immersed into the electrolyte as cathode, and the titanium mesh was used as anode. A constant DC current with density of 2 A/m^2 was applied to the two electrodes and powered with the duration of 2.5 h so that the amount of charge passed through the electrodes reached about 18 kC/m^2 carbon fiber surface. Afterwards, the power supply was disconnected and the cathode was cleaned with deionized water to obtain an electroplated CFT.

2.2.2. Preparation of the slurry impregnation

The impregnation treatment was performed in a setup (see the lower part in Fig. 1) developed at RISE (Sweden). It allows a continuous impregnation of CF bundle with viscous slurries. The setup consists of a fiber spreading unit and a 3-roller arrangement, which ensures a good impregnation throughout the bundle.

Before the preparation of geopolymer slurry, the Kaolin was calcined for 3 h at 800 °C to obtain metakaolin as the precursor. The waterglass solution was prepared by slowly adding NaOH into a silica solution to get a SiO_2/Na_2O molar ratio of 1 and a silica concentration of 3.3 mol/L. Metakaolin was added into the solution to achieve a final SiO_2/Na_2O molar ratio of 1.4. The impregnated bundle was cured at room temperature for 72 h and followed by 4-h curing at 80 °C (Bachinger et al., 2021b).

The TEOS, ethanol and deionized water were mixed with a ratio of 1/8/4 to produce a TEOS-solution. The pH of solution was then adjusted to 1.0 by the addition of HCl acid. The VTMOS-solution consisted of 2.7 mL TEOS, 4.7 mL HNO_3 (0.05 mol/L), 3.6 mol VTMOS and 1 mL MEMO. The impregnated bundles were cured at 70 °C for 24 h. More details can be found in a thesis (de Muinck, 2020).

2.2.3. Plasma treatment

The plasma treatment was performed in a vacuum plasma chamber (440 Plasma System, Technics Plasma GmbH, Germany) in the presence of oxygen gas. The treatments were performed at an oxygen gas pressure of 0.7 mbar and a plasma power of 320 W for 1 min.

2.2.4. Preparation of slag-based mortar

The alkali-activated mortar was mixed with the proportion shown in Table 3. The mortar was mixed according to the standard EN 196-1. All samples were cast and cured under room temperature (about 20 °C). Samples for pull-out test were prepared in coffee mugs where the impregnated bundles were kept in place (straight and ~0.5 cm above the bottom) by a plastic coffee mug lock. The mortar was cast in the coffee mug before it was sealed for embedding the fiber bundles. The samples were then stored in a sealed box with a wet cloth underneath for maintaining a high moisture environment with about 95% relative humidity (see Fig. 2). Water was added to the cloth for increasing the moisture content after 24 h. The wet cloth was taken away and the samples were demoulded after 7 d. Samples were stored in a moist box for an additional 2 d. Afterwards, samples were taken out and stored at lab room for 1 week before the pull-out test.

The composite specimens for bending test were cast in a steel mould with a size of 40 mm × 40 mm × 160 mm. The mould was firstly filled with mortar to a height of 5 mm and followed with a vibration. After that, CFT with a size of 40 mm × 160 mm was horizontally put on the surface. The mould was then filled with mortar to about 2/3 of the height, and it was vibrated to an even thickness. Finally, the rest volume of mould was filled with mortar and vibrated. The specimens were covered with a thick plastic sheet for 24 h before demoulding. Specimens were cured in the moist condition (water curing) to 7 d and 28 d, respectively.

Table 3
Mix proportion for alkali-activated slag mortar.

Materials	Density (kg/m^3)	Mass (kg/m^3)	Volume portion
Slag (Merit 5000)	2920	390	13.2%
Cement (CEM II/A-LL, 42.5R)	3088	97.5	3.1%
Gypsum ($CaSO_4{\cdot}2H_2O$)	2320	19.5	0.8%
Natural aggregate (0–10 mm)	2650	1500	56.5%
Water glass (Mr = 1.0, solid 30%)	1270	172	15.8%
Water	1000	108	10.6%

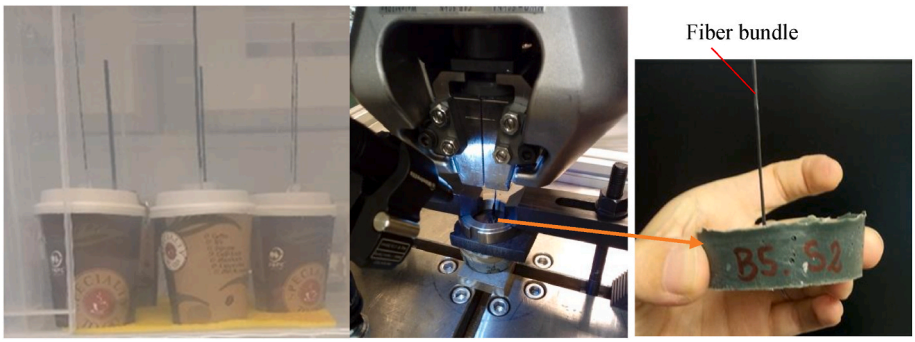

Fig. 2. The samples for pull-out test and the setup for measuring the pull-out strength.

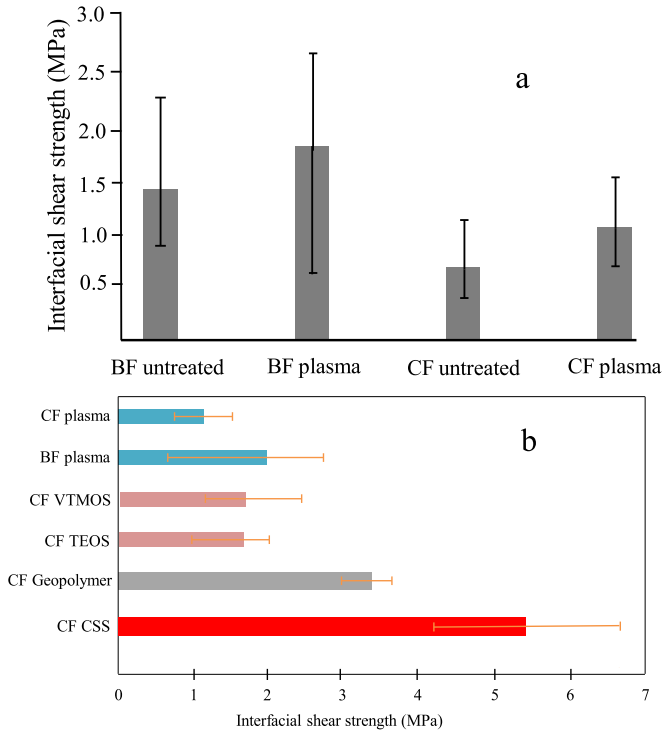

Fig. 3. The interfacial shear strength between fiber bundle and matrix: a – the comparison of the untreated and the plasma treated fiber bundles; b – the comparison in fibers with different treatment methods (an average value from 3 repeated tests).

2.3. The pull-out test

The pull-out strength between the matrix and the fiber bundles was tested by an AG-XK plus Shimadzu machine with a 50 kN grip at a speed of 1 mm/min. Fig. 2 shows the setup used to fix the samples. A rubber material was placed between the grips and mortar to avoid strong pressing stress. To reduce slippage, the fiber bundles were held between two tabs glued with P800 sandpaper.

The perimeter of the bundles (P) was initially characterized by a microscopy. The 3D scanning was used to evaluate the perimeter at different locations of the sample as well, and the detailed description of this measurement can be found in a previous work (de Muinck, 2020). The interfacial shear strength (τ) was calculated with the P, the embedded length (L) and the pull-out force (F) at the first peak of loading curve by the equation:

$$\tau = \frac{F}{P \times L} \quad (1)$$

2.4. The bending test

The flexural strength of the CFT reinforced mortar was tested on a three-points bending machine according to EN 196-1. The bending machine will automatically stop after a certain deformation, implying the formation of macro-cracks in the specimen. The load at this stop is usually used as the flexural strength of mortar. However, in this study the specimen was repeatedly placed on the machine for loading again until it was totally broken. After each stop, the maximum load was noted down and the width of the main crack (the largest one if there were many cracks) were measured using a digital microscope.

2.5. Backscatter scanning electron microscope

The CFT reinforced mortars were crushed into fragments, and then some small pieces embedded with CFT were chosen to be vacuum dried at 60 °C. The electroplated CFT and the dried pieces were vacuum embedded with a low viscosity epoxy. After it was hardened, all specimens were polished with a series grade of SiC papers from 800 meshes to 2000 meshes before they were polished with the diamond crystallites from 3 to 0.25 μm. The polished samples were plated with gold and examined by a scanning electron microscope (Nova NanoSEM 450, 14001-2004, America) under the backscatter scanning electron mode (BSE) with an accelerating voltage of 10 kV. The machine was coupled with an energy dispersive X-ray spectrometer for mapping of elements.

3. Results

3.1. Pull-out strength

Fig. 3 presents the interfacial shear strength between the matrix and fiber bundle (Bachinger et al., 2021a, 2021b). The shear strength between the BF bundle and mortar is higher than that of the untreated CF bundle. The plasma treatment induces a 40% and 65% increase in the shear strength of the commercial BF and CF bundle in matrix (see Fig. 3a), respectively. The plasma treating improves the adhesion between the CF and the matrix because it induces the formation of various functional groups on the fibers surface (carbonyl and hydroxyl) (Zielke et al., 1996; Dilsiz and Wightman, 1999; Sharma et al., 2014). These reactive functional groups will enhance the wettability of fiber surface and the physical intermolecular bonding with matrix (Bismarck et al., 2000; Montes-Morán et al., 2001). An increase in the shear strength between the plasma treated BF and matrix is due to the increase in surface roughness (Wang et al., 2007) and the generation of some active surface functionals groups (Khandelwal and Rhee, 2020).

The CF bundles impregnated in VTMOS-solution and TEOS-solution have a similar shear strength in the AAS matrix (see Fig. 3b), and their shear strength is about 70% higher than that of the plasma treated CF. TEOS was also used in the investigation (Lu et al., 2018) to graft SiO_2 on the surface of CF, and there was an effective connection between CF and

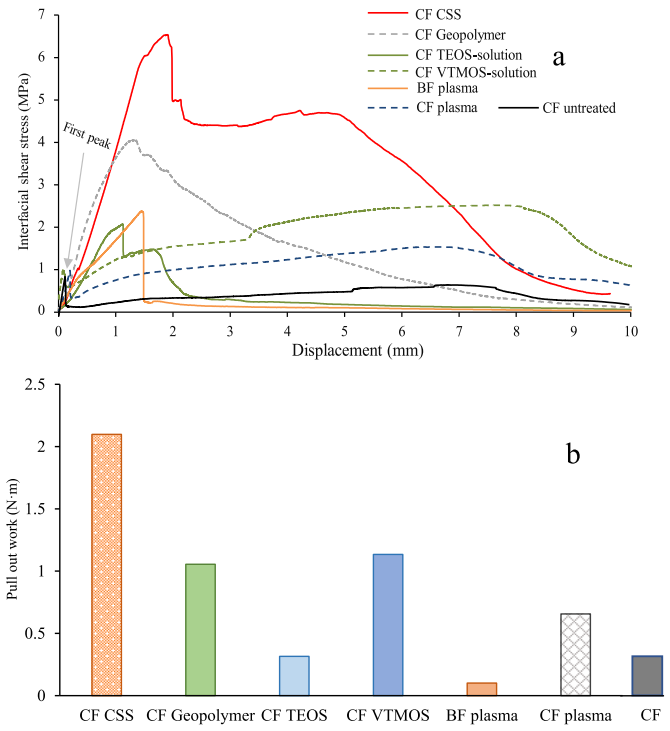

Fig. 4. The typical strength-displacement curve (a) and the pull-out work of the fiber bundles (b).

silica built by TEOS. TEOS also interacts with the hydration products (portlandite and calcium silicate hydrate) (Barberena-Fernández et al., 2015), so the interfacial strength between CF and matrix has been improved by the TEOS impregnation. VTMOS-solution comprises VTMOS, TEOS and MEMO, and the further addition of TEOS and MEMO is mainly functioned to adjust the ratio of alkyl and oxygenated functional groups (Metroke et al., 2004). It seems that this modification has few effects on the interfacial shear strength. An impregnation in geopolymer slurry has a greater improving in the shear strength than TEOS and VTMOS-solution. The interfacial shear strength of CF impregnated with geopolymer is about 4.5 times higher than the value of untreated CF. The CSS electroplated CF has the highest interfacial shear strength in AAS matrix, and the value is almost 7.2 times higher than the untreated CF and 5 times higher than that of the plasma treated CF.

Fig. 4 shows the detailed strength-displacement curves and the pull-out work of different fiber bundles. The pull-out of fiber bundle includes three failure modes: the breaking of bond between the matrix and fibers, peeling of the composites at the interface and the slipping of the fibers (de Felice et al., 2014). The debonding failure corresponds to a sharp drop of the force after the first peak, and it is a linear stage before the debonding at interface due to the elastic stretching of the carbon fibers (Lu et al., 2018) (also see Fig. 4a). After the first peak, the pull-out force is dominated by the frictional force. The stress would decrease linearly upon displacement, assuming that there is no peeling of composites. However, an increase of force is observed in the plasma-treated and VTMOS-solution treated fibers, defined as slip hardening from the jamming effect of fibers (Redon et al., 2001). The pull-out of the plasma treated BF and TEOS-solution treated CF shows a slip softening. It is probably due to the phenomenon that the fiber surface becomes smooth after a sudden damage of bond between the connection between fiber yarn and matrix, so the force presents a sharp decrease during the

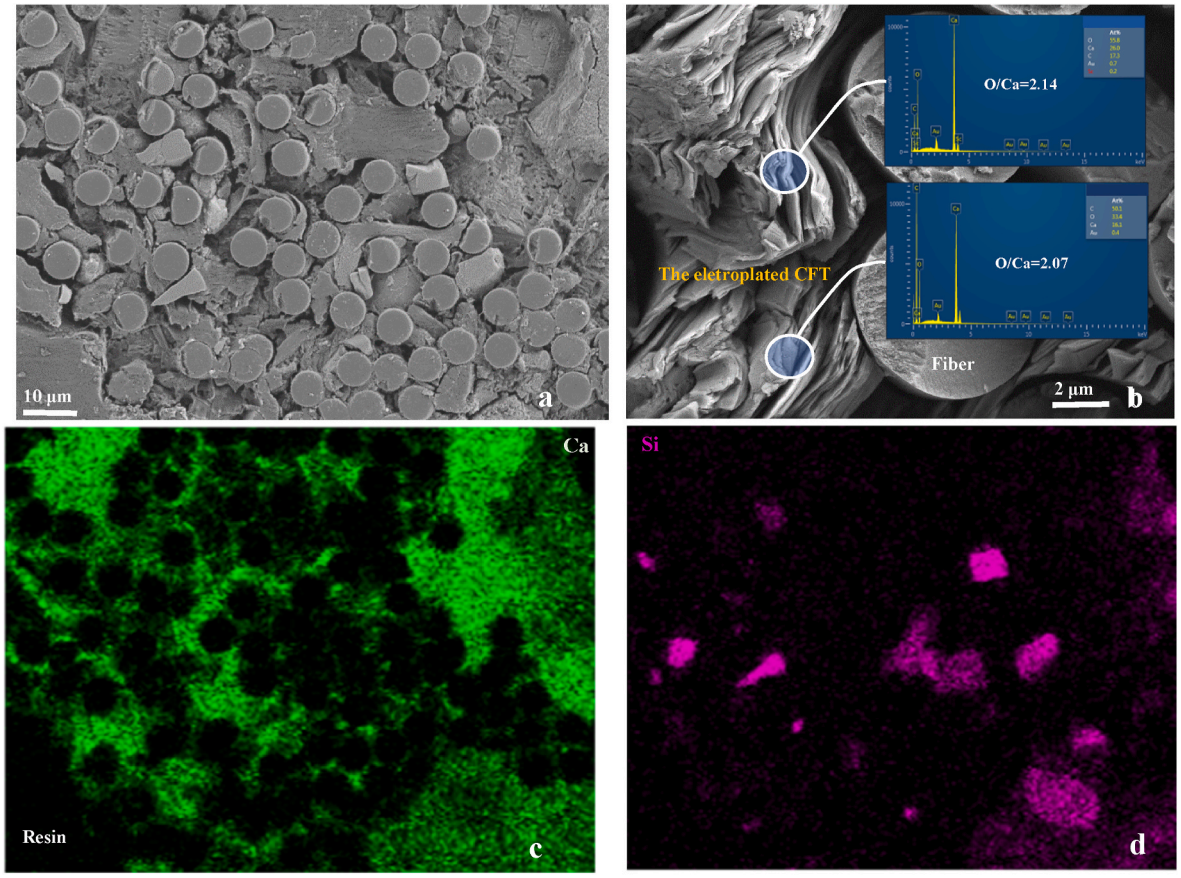

Fig. 5. The BSEM images and the elements map of the cross section of the CSS electroplated CFT.

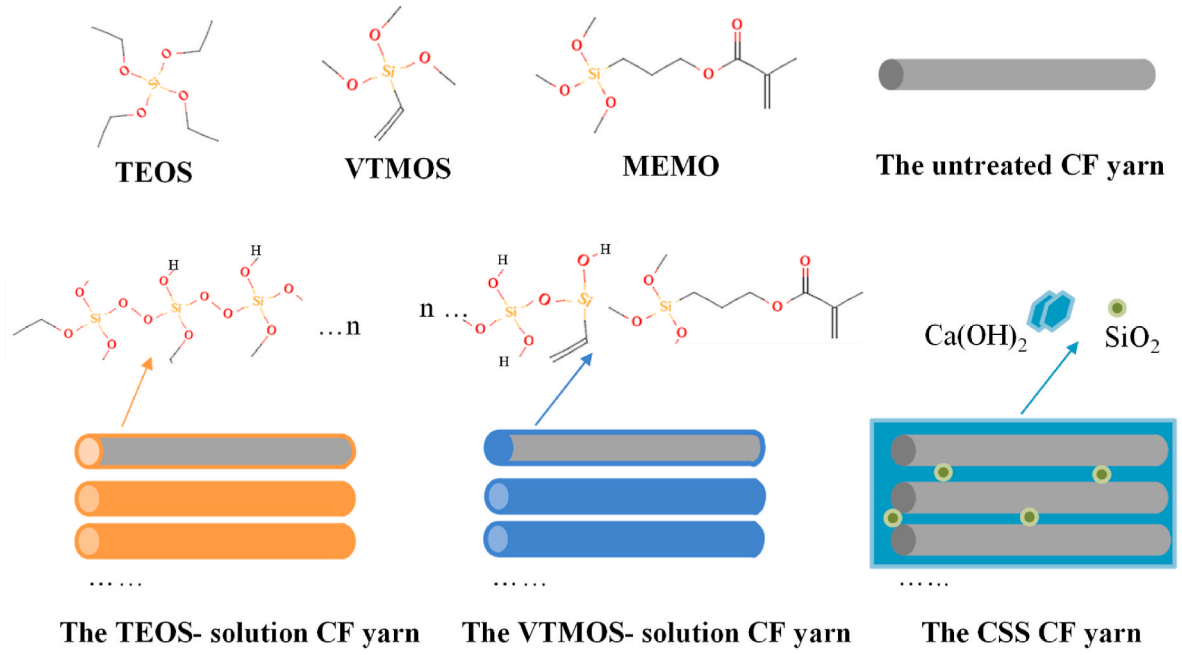

Fig. 6. Illustration of the surface feature of CF after different treatments.

slipping. The impregnation by geopolymer can largely enhance the bond as well as the frictional force at the interface. The electroplating by CSS results in not only the highest bond force but also the strongest frictional force. The CSS treated CF bundle also presents a slip hardening effect after the debonding process. This hardening process may be caused by increase in frictional surface area from the pilling of the plated substance.

To assess the energy absorption capacity, the pull-out work (W, N·m) was calculated by the integration of force-displacement curve (Eq. (2)) with the loading force value ($F(x)$, N) at corresponding displacement (x, m) (Oh et al., 2021). It indicates the consumption of energy for a complete pull-out of fiber bundles with a similar embedded length (L, m).

$$W = \int_0^L F(x)dx \tag{2}$$

Fig. 4b shows that although the plasma treated BF has a higher interfacial strength (Fig. 4a), it consumes the lowest energy before a full pull-out. The TEOS treatment has negligible effects on the pull-out work, but the plasma treatment and impregnation by VTMOS-solution induce a significant enhancement in the pull-out energies. The pull-out work of the geopolymer treated and CSS electroplated CF is about 3 and 7 times higher than that of the untreated CF, respectively.

3.2. The surface of the treated CF

The CF electroplated with CSS has the best bonding performance among CF bundles with different treatment methods. Therefore, the further analysis will be focused on revealing its surface feature characterized by the BSE. Fig. 5a shows that the gap between the fibers has been filled with the electroplated substance. An element analysis at the high magnification (see Fig. 5b) demonstrates that the substance is rich of Ca and with the O/Ca molar ratio of about 2, so the main substance is most likely portlandite. The electrochemical oxidation of carbon fibers occurs in the sodium hydroxide solution with the production of sodium phenoxides (Gulyás et al., 2001). Therefore, the electrochemical reactions would also occur on the surface of cathode during the electroplating treatment in CSS, possibly resulting in a formation of bond between portlandite and carbon fiber.

The micro-sized portlandite layer wraps around the CF yarns after

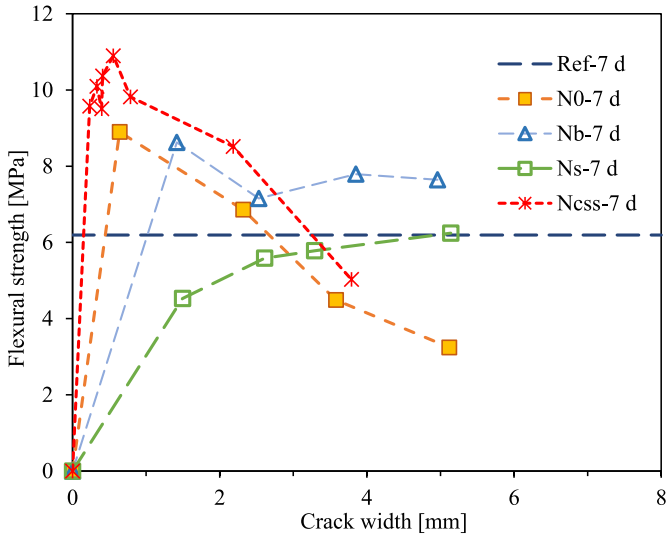

Fig. 7. The flexural strength-crack width curve of the alkali-activated slag mortars at 7 d after cyclic loading: the untreated CFT (N0), the basalt fiber textile (Nb), the SBR-impregnated CFT (Ns) and the CSS electroplated CFT reinforced (Ncss) mortar. Note that the reference mortars without CFT (Ref-7 d) were completely broken into two parts after the first loading.

the CSS treatment. The map of Ca and Si elements illustrates that majority of the coated material is portlandite, but it also consists of some silicates. Silica colloids in solution normally have a negative surface charge so the nano-silica will be coated on the anode (Li et al., 2020). However, the pH in the solution will increase as the dissociation of water under the electrifying, and the increasing pH will probably induce the formation of $Ca(H_3SiO_4)^+$ and $Ca(H_2SiO_4)$ in solution (Huang et al., 2022). Therefore, the precipitation of calcium silicate hydrate can occur on the cathode surface as well.

Fig. 6 illustrates the molecular structure of organic precursors used in the solution treatment of CF. The hydrolysis of TEOS will take place in the acid solution, and then the reaction will proceed with the sol-gel polymerization of the hydrolyzed TEOS (Ng and McCormick, 1996;

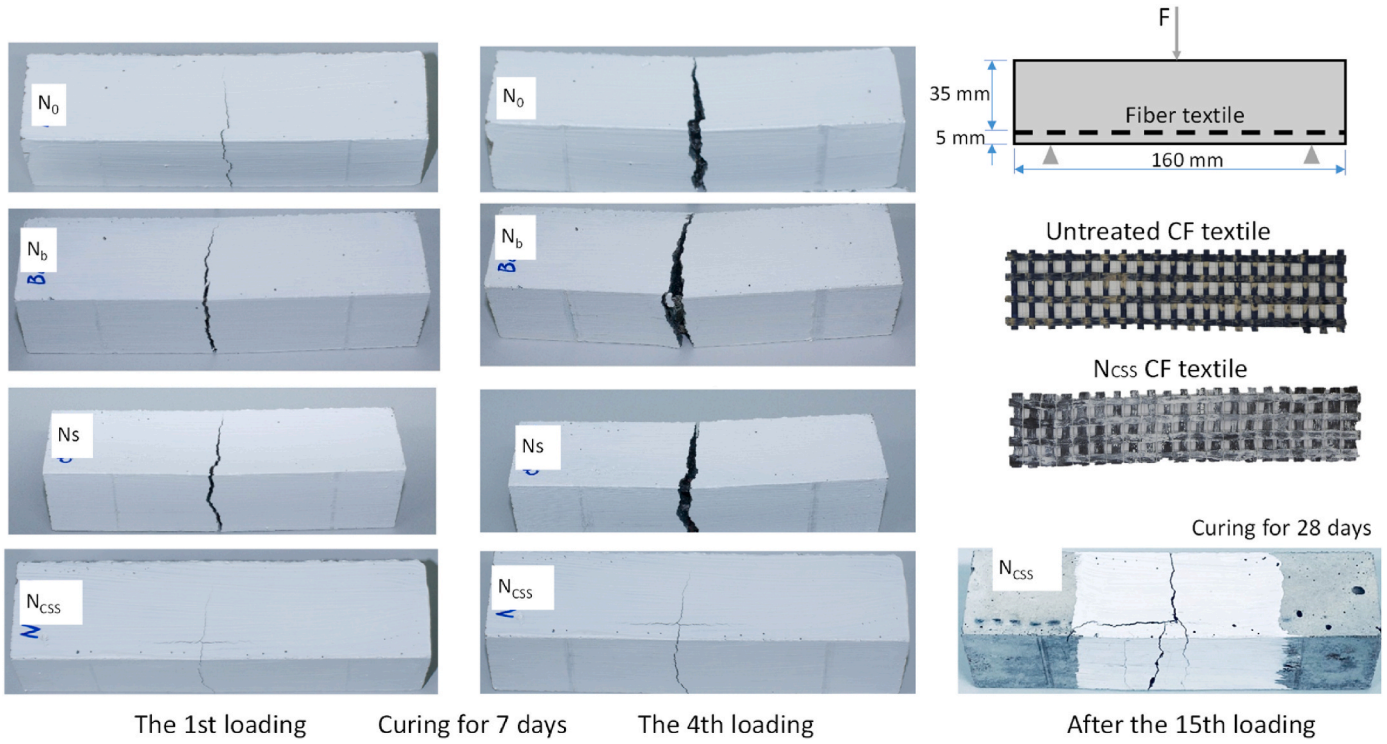

Fig. 8. The typical feature of the cracks and shape of the CFT reinforced mortars after the cyclic bending test: the untreated CFT (N0), the basalt fiber textile (Nb), the SBR-impregnated CFT (Ns) and the CSS electroplated CFT reinforced (Ncss) mortar with curing time of 7 and 28 d.

Tamon et al., 1998). A layer of the silica gel will be coated on the surface of the CF yarns. The addition of VTMOS and MEMO changes the length of alkyl on the surface the coated matter (Metroke et al., 2004), so it may induce different effects on the bonding strength. It can be observed from the pull-out curves (see Fig. 4) that VTMOS-solution treated CF bundle has a higher frictional strength, resulting in a higher pull-out work compared with TEOS. CF yarns with CSS electroplating will be bound together by the coated substance (portlandite and silicate). These coatings enhance the chemical bonding as well as the frictional forces between CF bundles and ASS matrix.

3.3. *The flexural strength of CFT mortar under the cyclic loading*

The use of fibers and textile mitigates the brittle nature of AAS mortar by enhancing the tensile strength, ductility and toughness (Koutas et al., 2019). The performance of fiber reinforced composites under cyclic loading is significant for minimizing the damage from the catastrophic disasters such as highway bridge collapses and earthquakes (Bontea et al., 2000; Howser et al., 2011). Fig. 7 presents the flexural strength and maximum width of cracks in CFT reinforced mortar under the cyclic loading at the curing age of 7 d. The reference mortar without fibers (Ref-7d) was broken at the first load with an average flexural strength of 6.2 MPa. The AAS mortar with the SBR-impregnated CFT (commercial) has a lower flexural strength at the first loading than the reference mortar, but a hardening phenomenon has been detected after the repeated loading. Mortar reinforced with the untreated CFT has a similar flexural strength as the mortar with BF textile (commercial) at the first load, but the BF textile has a better inhibiting effect on the decay of the strength under cyclic loading. Mortar reinforced with CSS electroplated CFT has the highest flexural strength at the first load, with an increase by 22.5% for the maximum force compared with untreated CFT. Moreover, the flexural strength shows an increase by 13% after four cyclic loadings. The CSS electroplated CFT has a significant effect on the inhibiting of crack growth. The maximum crack width in mortar with the CSS coated CFT (Ncss-7d) is only 0.55 mm after the fourth

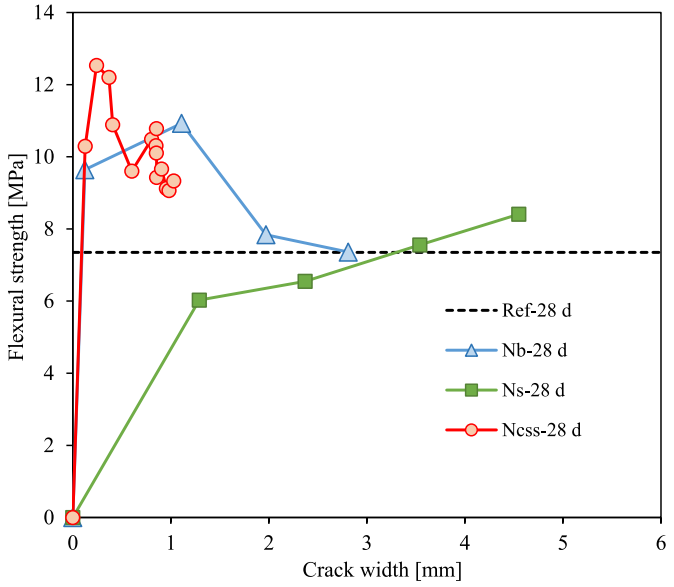

Fig. 9. The flexural strength-crack width curve of CFT reinforced mortars at 28 d with a cyclic loading. A comparison between the CSS electroplated CFT (Ncss) and commercial fiber textile (Nb and Ns).

loading, and this is much smaller that the cracks in mortar reinforced with the untreated CF (N0) and commercial textiles (Nb and Ns).

Fig. 8 illustrates the loading direction and typical features of the cracks after the bending test. There is a severe crack in the middle of the Nb and Ns prism with a width of 1.4–1.5 mm after the first bending test. Ncss prism has two fine cracks distributed in two perpendicular directions. The occurrence of the horizontal crack is due to the transferring of the tensile force to vertical direction by the CSS treated CFT. The widths of cracks in N0, Nb and Ns have a significant increase after four

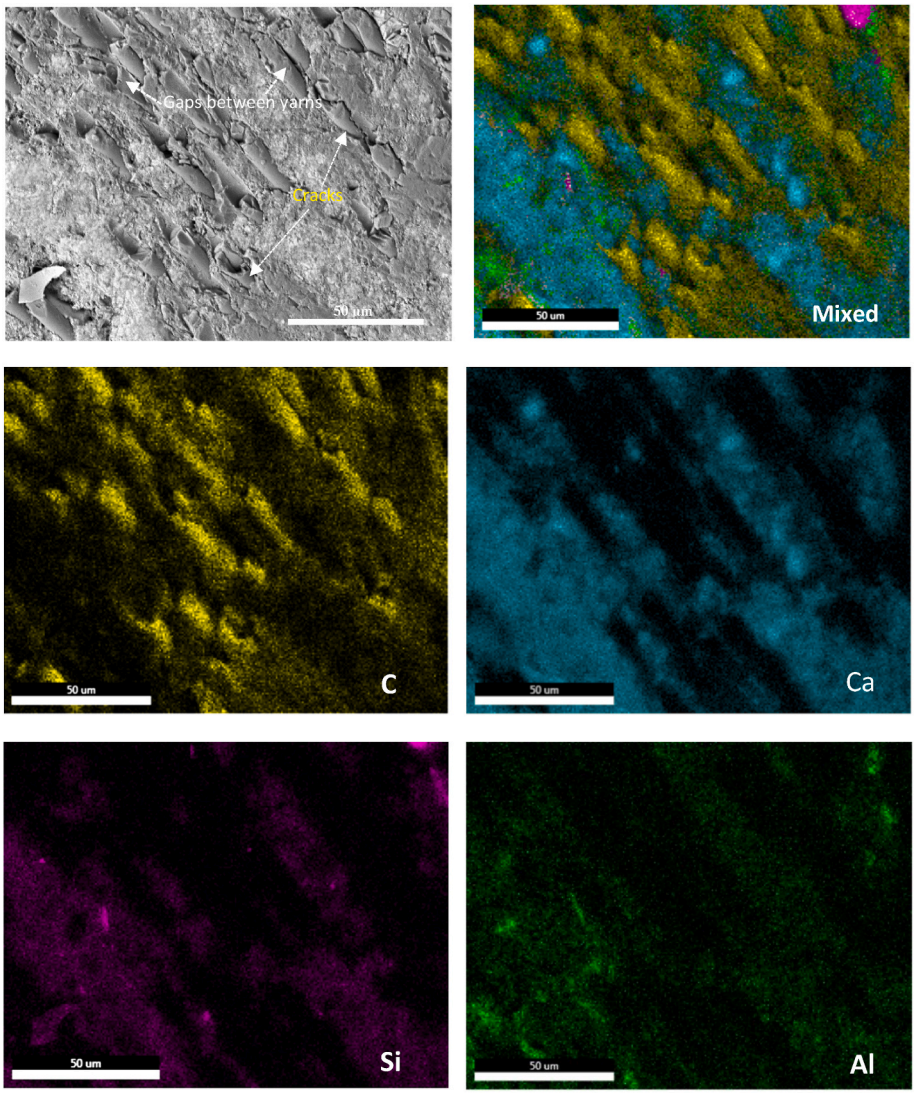

Fig. 10. The BSE images and the elements map of interfacial zone between the untreated CFT and the alkali-activated slag mortar cured for 7 d.

cyclic tests, but the crack in Ncss sample is still very small. After curing for 28 d, the maximum bending force seems to be increased by 30% through the CSS treatment. Moreover, Ncss prism maintains in a good shape after 15 cyclic tests with a maximum crack width of 0.9 mm (see Figs. 8 and 9). The longer curing time induces a higher flexural strength at the first test for all the samples, but it seems to have very weak influence on the propagation of crack in the commercial CFT reinforced mortar (Nb and Ns). The CSS treated CFT has a better inhibiting effect on the crack growth after a longer curing time, which will be further discussed in the next section.

The bending performance of the textile reinforced mortar is mainly controlled by the bonding between the matrix and textiles (Carozzi and Poggi, 2015; Raoof et al., 2016). Many factors make impact on the bonding strength between textile and matrix: the mechanical performance of both textile and matrix, the penetrate capability of mortar into the grid and the frictional force between the filaments. Fig. 8 shows that the electroplating in CSS has coated some materials on the CF surface but without filling the grids. This treatment also fills the gaps between the fiber yarns to bind them together (see Fig. 5). These effects induce an increase in the chemical bond and the frictional force between CFT and AAS mortar (See Fig. 4), resulting in the best reinforcement in the bending performance.

3.4. Interfacial feature of CFT in mortars

The analysis of microstructure by the scanning electron microscopy under backscatter mode is an effective way to indicate the interfacial features (phases and cracking) of the concrete composites (Huang et al., 2019, 2020). Fig. 10 shows the BSE images of the untreated CFT reinforced AAS mortar at 7 d. The attention is paid to the interfacial zone between the fiber bundle and the hardened paste matrix. Pastes have penetrated in gaps between different fiber bundles, but some gaps remain empty between the yarns. Many microcracks can be observed in the interfacial transition zone between the untreated yarns and the matrix. Some investigation (Katz et al., 1995) also found that the surface of the untreated carbon fiber was very smooth and clean from particles after being pulled out from the matrix, which implied a poor bond between the matrix and fibers. The elements map can clearly distinguish the fibers and matrix. It shows that Ca, Si, and Al are the primary elements in the penetrated pastes. The main end-phase in the hydration products of slag (based on composition in Table 1) is composed of C-(N-)A-S-H gel, Mg-Al LDH and strätlingite (Myers et al., 2017), which explains the observed distribution of elements.

Fig. 11 presents the BSE images and the elements map of the AAS mortar reinforced with CSS electroplated CFT. The mixed elements map is useful for distinguishing the carbon fibers, the electroplated Ca-rich

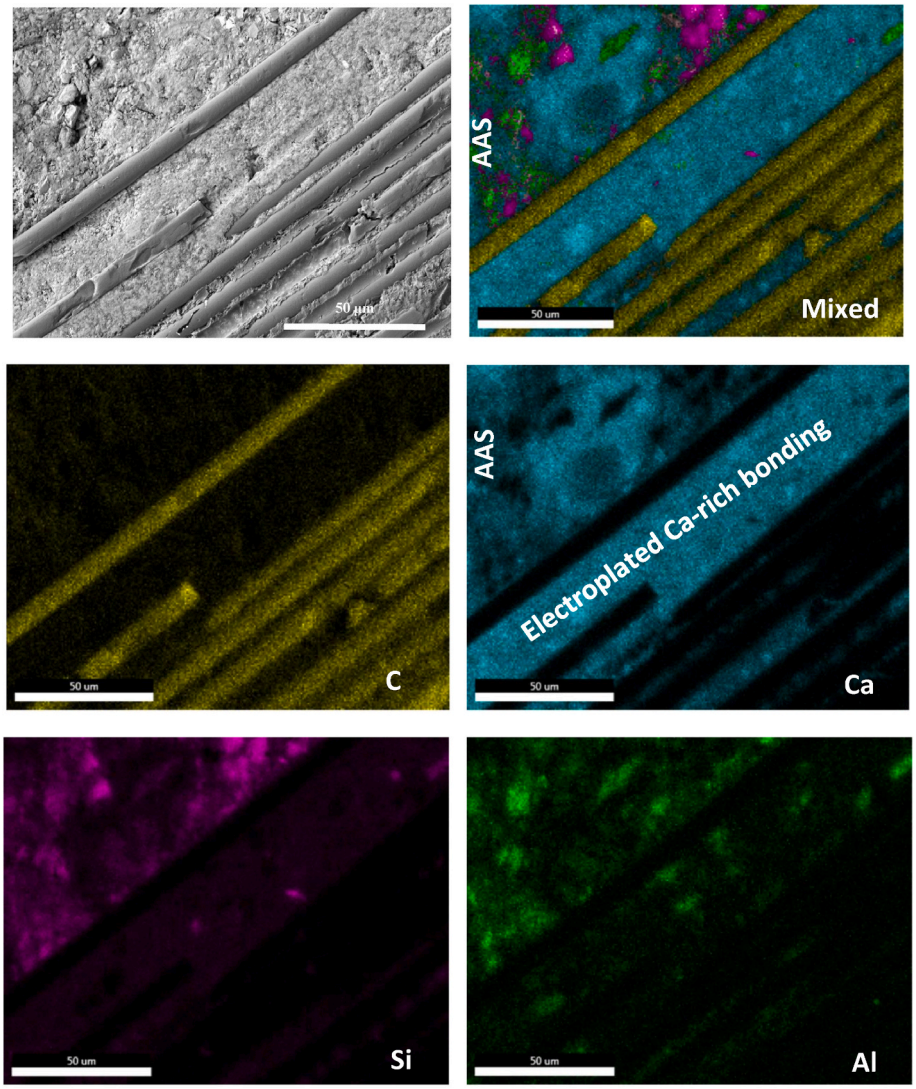

Fig. 11. The BSE images and the elements map of interfacial zone between the CSS electroplated CFT and the alkali-activated slag mortar at 7 d.

substance and AAS paste. The fiber yarns are densely bond together with the electroplated portlandite, which has been detected in the bundles before mixing into AAS (see Fig. 5). The electroplated matter is much denser than the penetrated pastes (see Fig. 10). The AAS paste merges seamlessly with the electroplated portlandite, without an apparent interfacial transition zone between them. Moreover, the CSS electroplated CFT exhibits a denser interfacial zone than the untreated CFT in AAS mortar, due to the strong bonding between carbon fiber and portlandite under the electrified condition. Therefore, The CSS treatment CFT yields the highest flexural strength of reinforced mortar, and more notably, exhibits the most inhibiting effective on the crack propagation (see Fig. 7). The Si-rich substance accumulate in some local region on the surface of electroplated CFT (see the mixed element map), and there is few Si element in the gap between fiber yarns at 7 d.

After curing for 28 d (see Fig. 12), the difference between the electroplated substance and AAS pastes becomes more evident in elements map compared with the mortar at 7 d. The interfacial zone between CFT and the coated Ca-rich substance remains a dense feature. Moreover, the Si rich substance penetrated in the gaps of fiber yarns with an even distribution. This is most possibly due to the hydration reaction between the electroplated portlandite and the slag after a long-time curing (Kolani et al., 2012). The later age reaction increases the strength of AAS mortar and builds a stronger connection between CFT and the matrix, so it will cause an increase in the flexural strength and an enhancement in inhibiting effects on the crack propagation (see Figs. 7–9).

4. Conclusions

The embedding of CFT can mitigate the brittle weakness of the AAS mortar. The effect of various treatment methods on the performance of mortar with textile was identified by pull-out tests, flexural strength test and scanning electron microscope. The main conclusions from this investigation are presented as follows.

All of the treatments in this study effectively improve the interfacial shear strength between fiber bundles and AAS matrix, including the plasma, slurry impregnation and electroplating treatments. A plasma treatment induces some active functional groups on the fiber surface to increase the bonding strength between AAS matrix and fiber bundles (CF and BF). The impregnation in TEOS and VTMOS solutions induces an increase in shear strength between fibers and matrix. The geopolymer impregnation increases the interfacial shear strength by about 350%, and the CSS electroplating treatment has the best effect on bonding strength with an increase by 620%. After the electroplating, a dense layer of portlandite particles was deposited on the surface of the CF fiber yarns and within the gaps to interconnect the yarns. The CSS electroplating enhances not only the chemical bonding but also the friction between CF bundles and matrix.

The flexural strength of the CFT reinforced AAS mortar has been

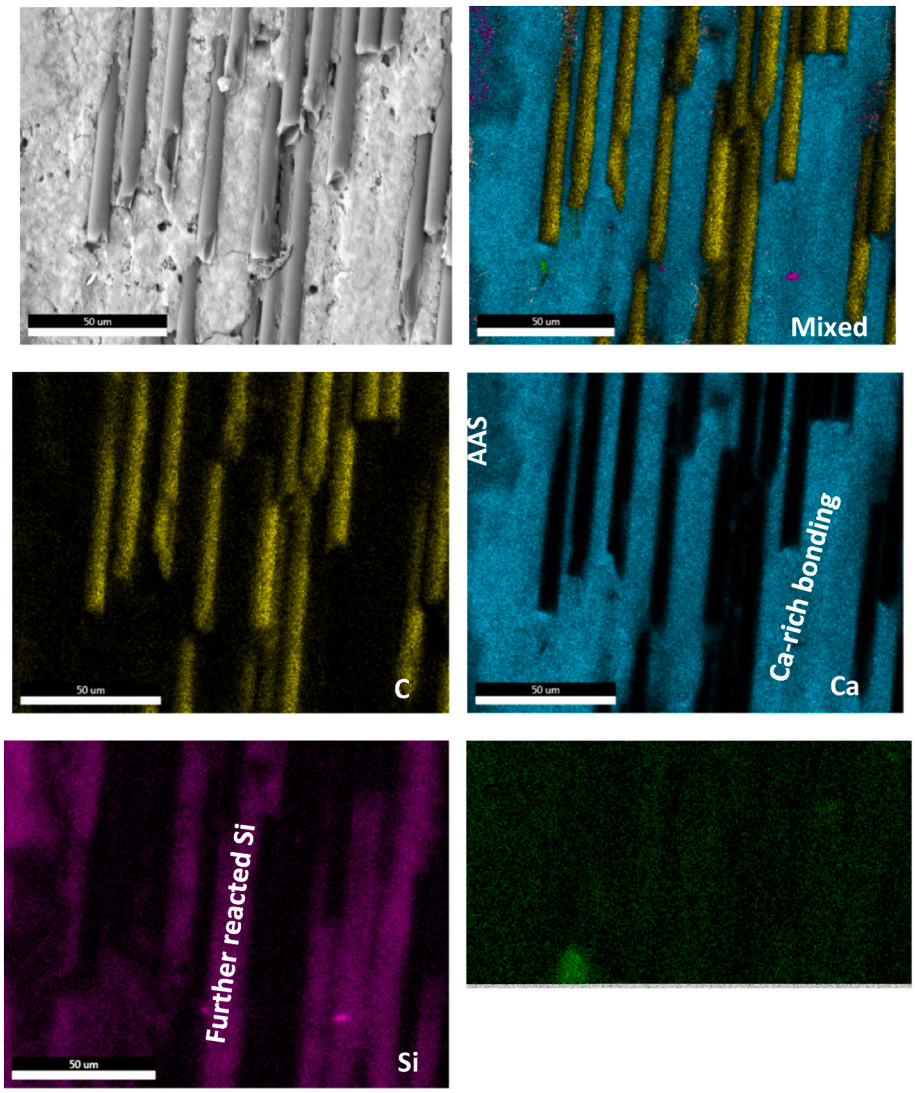

Fig. 12. The BSE images and the elements map of interfacial zone between the CSS electroplated CFT and the alkali-activated slag mortar at 28 d.

improved by the electroplating treatment of CFT. After a CSS treatment of CFT, the maximum bending load has been increased by 22.5% and 30% at 7 d and 28 d, respectively. The use of CSS electroplated CFT also shows a much better inhibiting effect on crack propagation under cyclic loading compared with the untreated and commercial CFT, which becomes more significant as the curing age increases. The width of the micro-crack in mortar with CSS electroplated CFT is smaller than 0.9 mm even after 15 cyclic bending tests. CSS electroplating treatment avoids the formation of cracks between the fiber yarns and matrix, and builds a denser connection between fibers compared with the penetrated paste, so it can induce a good enhancement in the bonding strength in matrix. The Si-rich phase can penetrate in the plated substance due to the further reaction of slag and portlandite. This enforces a better inhibiting effect on the crack propagation after a longer curing time.

CRediT authorship contribution statement

Liming Huang: Methodology, Formal analysis, Writing – original draft, Writing – review & editing. **Luping Tang:** Methodology, Experiments, Writing – review & editing, Supervision, Project administration, Funding acquisition. **Angelika Bachinger:** Investigation, Writing – review & editing. **Yongqiang Li:** Experiments, Formal analysis. **Zhenghong Yang:** Writing – review & editing, Supervision, Project administration.

Declaration of competing interest

We declare that we have no known competing financial interests or personal relationships that could have appeared to influence the work reported in this paper.

Data availability

Data will be made available on request.

Acknowledgements

The authors appreciate the financial support from Swedish VINNOVA (No. 2016–03367; 2021–04033) and National Key Research and Development Program of China (No. 2018YFD1101002). Appreciations are also given to Derk de Muinck, Peter Hellström, Anaïs Domergue, and Laurie Gaüzere for their helps in the fiber treatments and the pull-out measurements.

References

Amran, M., Fediuk, R., Abdelgader, H.S., Murali, G., Ozbakkaloglu, T., Lee, Y.H., Lee, Y. Y., 2022. Fiber-reinforced alkali-activated concrete: a review. J. Build. Eng. 45, 103638 https://doi.org/10.1016/j.jobe.2021.103638.

Aydın, S., Baradan, B., 2013. The effect of fiber properties on high performance alkali-activated slag/silica fume mortars. Compos. B Eng. 45, 63–69. https://doi.org/10.1016/j.compositesb.2012.09.080.
Bachinger, A., Hellström, P., de Muinck, D., 2021a. Commercial Textile Reinforcements–Performance in Green Cement and Surface Treatment.
Bachinger, A., Hellström, P., Domergue, A., Gaüzere, L., de Muinck, D., 2021b. Development of Textile Reinforcements with Improved Adhesion and Thermal Stability for Green Cement.
Barberena-Fernández, A.M., Carmona-Quiroga, P.M., Blanco-Varela, M.T., 2015. Interaction of TEOS with cementitious materials: chemical and physical effects. Cem. Concr. Compos. 55, 145–152. https://doi.org/10.1016/j.cemconcomp.2014.09.010.
Behfarnia, K., Rostami, M., 2017. Mechanical properties and durability of fiber reinforced alkali activated slag concrete. J. Mater. Civ. Eng. 29, 04017231 https://doi.org/10.1061/(ASCE)MT.1943-5533.0002073.
Bernal, S., De Gutierrez, R., Delvasto, S., Rodriguez, E., 2010. Performance of an alkali-activated slag concrete reinforced with steel fibers. Construct. Build. Mater. 24, 208–214. https://doi.org/10.1016/j.conbuildmat.2007.10.027.
Bismarck, A., Richter, D., Wuertz, C., Kumru, M.E., Song, B., Springer, J., 2000. Adhesion: comparison between physico-chemical expected and measured adhesion of oxygen-plasma-treated carbon fibers and polycarbonate. J. Adhes. 73, 19–42. https://doi.org/10.1080/00218460008029295.
Bontea, D.-M., Chung, D.D.L., Lee, G.C., 2000. Damage in carbon fiber-reinforced concrete, monitored by electrical resistance measurement. Cement Concr. Res. 30, 651–659. https://doi.org/10.1016/S0008-8846(00)00204-0.
Brameshuber, W., 2006. Report 36: Textile Reinforced Concrete-State-Of-The-Art Report of RILEM TC 201-TRC. RILEM publications.
Carozzi, F.G., Poggi, C., 2015. Mechanical properties and debonding strength of Fabric Reinforced Cementitious Matrix (FRCM) systems for masonry strengthening. Compos. B Eng. 70, 215–230. https://doi.org/10.1016/j.compositesb.2014.10.056.
Choi, J.-I., Nguyễn, H.H., Cha, S.L., Li, M., Lee, B.Y., 2021. Composite properties of calcium-based alkali-activated slag composites reinforced by different types of polyethylene fibers and micromechanical analysis. Construct. Build. Mater. 273, 121760 https://doi.org/10.1016/j.conbuildmat.2020.121760.
Chung, D.D., 2016. Carbon Composites: Composites with Carbon Fibers, Nanofibers, and Nanotubes. Butterworth-Heinemann.
Cui, H., Feng, T., Yang, H., Bao, X., Tang, W., Fu, J., 2018. Experimental study of carbon fiber reinforced alkali-activated slag composites with micro-encapsulated PCM for energy storage. Construct. Build. Mater. 161, 442–451. https://doi.org/10.1016/j.conbuildmat.2017.11.075.
de Felice, G., De Santis, S., Garmendia, L., Ghiassi, B., Larrinaga, P., Lourenço, P.B., Oliveira, D.V., Paolacci, F., Papanicolaou, C.G., 2014. Mortar-based systems for externally bonded strengthening of masonry. Mater. Struct. 47, 2021–2037. https://doi.org/10.1617/s11527-014-0360-1.
de Muinck, D., 2020. Improving Adhesion between Carbon Fibre Reinforcements and Alkali-Activated Cements. (Master Thesis). Chalmers University of Technology.
Dilsiz, N., Wightman, J.P., 1999. Surface analysis of unsized and sized carbon fibers. Carbon 37, 1105–1114. https://doi.org/10.1016/S0008-6223(98)00300-5.
Ding, Y., Dai, J.-G., Shi, C.-J., 2016. Mechanical properties of alkali-activated concrete: a state-of-the-art review. Construct. Build. Mater. 127, 68–79. https://doi.org/10.1016/j.conbuildmat.2016.09.121.
Gulyás, J., Földes, E., Lázár, A., Pukánszky, B., 2001. Electrochemical oxidation of carbon fibres: surface chemistry and adhesion. Compos. Part Appl. Sci. Manuf. 32, 353–360. https://doi.org/10.1016/S1359-835X(00)00123-8.
Howser, R.N., Dhonde, H.B., Mo, Y.L., 2011. Self-sensing of carbon nanofiber concrete columns subjected to reversed cyclic loading. Smart Mater. Struct. 20, 085031 https://doi.org/10.1088/0964-1726/20/8/085031.
Huang, L., Tang, L., Gu, H., Li, Z., Yang, Z., 2022. New insights into the reaction of tricalcium silicate (C_3S) with solutions to the end of the induction period. Cement Concr. Res. 152, 106688 https://doi.org/10.1016/j.cemconres.2021.106688.
Huang, L., Yang, Z., Li, Z., Xu, Y., Yu, L., 2020. Recycling of the end-of-life lightweight aggregate concrete (LWAC) with a novel approach. J. Clean. Prod. 275, 123099.
Huang, L., Yu, L., Zhang, H., Yang, Z., 2019. Composition and microstructure of 50-year lightweight aggregate concrete (LWAC) from Nanjing Yangtze River bridge (NYRB). Construct. Build. Mater. 216, 390–404.
Karunanithi, S., 2017. Experimental studies on punching shear and impact resistance of steel fibre reinforced slag based geopolymer concrete. Adv. Civ. Eng. 2017, 1–9. https://doi.org/10.1155/2017/9210968.
Katz, A., Li, V.C., Kazmer, A., 1995. Bond properties of carbon fibers in cementitious matrix. J. Mater. Civ. Eng. 7, 125–128. https://doi.org/10.1061/(ASCE)0899-1561(1995)7:2(125).
Khandelwal, S., Rhee, K.Y., 2020. Recent advances in basalt-fiber-reinforced composites: tailoring the fiber-matrix interface. Compos. B Eng. 192, 108011 https://doi.org/10.1016/j.compositesb.2020.108011.
Kolani, B., Buffo-Lacarrière, L., Sellier, A., Escadeillas, G., Boutillon, L., Linger, L., 2012. Hydration of slag-blended cements. Cem. Concr. Compos. 34, 1009–1018. https://doi.org/10.1016/j.cemconcomp.2012.05.007.
Koutas, L.N., Tetta, Z., Bournas, D.A., Triantafillou, T.C., 2019. Strengthening of concrete structures with textile reinforced mortars: state-of-the-art review. J. Compos. Construct. 23, 03118001 https://doi.org/10.1061/(ASCE)CC.1943-5614.0000882.
Li, H., Liebscher, M., Curosu, I., Choudhury, S., Hempel, S., Davoodabadi, M., Dinh, T.T., Yang, J., Mechtcherine, V., 2020. Electrophoretic deposition of nano-silica onto carbon fiber surfaces for an improved bond strength with cementitious matrices. Cem. Concr. Compos. 114, 103777 https://doi.org/10.1016/j.cemconcomp.2020.103777.
Li, V.C., Wu, C., Wang, S., Ogawa, A., Saito, T., 2002. Interface tailoring for strain-hardening polyvinyl alcohol-engineered cementitious composite (PVA-ECC). Mater. J. 99, 463–472.
Liu, S., Rawat, P., Chen, Z., Guo, S., Shi, C., Zhu, D., 2020. Pullout behaviors of single yarn and textile in cement matrix at elevated temperatures with varying loading speeds. Compos. B Eng. 199, 108251 https://doi.org/10.1016/j.compositesb.2020.108251.
López-Buendía, A.M., Romero-Sánchez, M.D., Climent, V., Guillem, C., 2013. Surface treated polypropylene (PP) fibres for reinforced concrete. Cement Concr. Res. 54, 29–35. https://doi.org/10.1016/j.cemconres.2013.08.004.
Lu, M., Xiao, H., Liu, M., Li, X., Li, H., Sun, L., 2018. Improved interfacial strength of SiO2 coated carbon fiber in cement matrix. Cem. Concr. Compos. 91, 21–28. https://doi.org/10.1016/j.cemconcomp.2018.04.007.
Meng, W., Khayat, K.H., Bao, Y., 2018. Flexural behaviors of fiber-reinforced polymer fabric reinforced ultra-high-performance concrete panels. Cem. Concr. Compos. 93, 43–53. https://doi.org/10.1016/j.cemconcomp.2018.06.012.
Metroke, T.L., Gandhi, J.S., Apblett, A., 2004. Corrosion resistance properties of Ormosil coatings on 2024-T3 aluminum alloy. Prog. Org. Coating 50, 231–246. https://doi.org/10.1016/j.porgcoat.2004.03.001.
Montes-Morán, M.A., Martínez-Alonso, A., Tascón, J.M.D., Young, R.J., 2001. Effects of plasma oxidation on the surface and interfacial properties of ultra-high modulus carbon fibres. Compos. Part Appl. Sci. Manuf. 32, 361–371. https://doi.org/10.1016/S1359-835X(00)00109-3.
Myers, R.J., Bernal, S.A., Provis, J.L., 2017. Phase diagrams for alkali-activated slag binders. Cement Concr. Res. 95, 30–38. https://doi.org/10.1016/j.cemconres.2017.02.006.
Nematollahi, B., Qiu, J., Yang, E.-H., Sanjayan, J., 2017. Micromechanics constitutive modelling and optimization of strain hardening geopolymer composite. Ceram. Int. 43, 5999–6007. https://doi.org/10.1016/j.ceramint.2017.01.138.
Ng, L.V., McCormick, A.V., 1996. Acidic Sol−Gel polymerization of TEOS: effect of solution composition on cyclization and bimolecular condensation rates. J. Phys. Chem. 100, 12517–12531. https://doi.org/10.1021/jp960089o.
Niş, A., Eren, N.A., Çevik, A., 2021. Effects of nanosilica and steel fibers on the impact resistance of slag based self-compacting alkali-activated concrete. Ceram. Int. 47, 23905–23918. https://doi.org/10.1016/j.ceramint.2021.05.099.
Oh, T., You, I., Banthia, N., Yoo, D.-Y., 2021. Deposition of nanosilica particles on fiber surface for improving interfacial bond and tensile performances of ultra-high-performance fiber-reinforced concrete. Compos. B Eng. 221, 109030 https://doi.org/10.1016/j.compositesb.2021.109030.
Park, J.-M., Kim, P.-G., Jang, J.-H., Wang, Z., Hwang, B.-S., DeVries, K.L., 2008. Interfacial evaluation and durability of modified Jute fibers/polypropylene (PP) composites using micromechanical test and acoustic emission. Compos. B Eng. 39, 1042–1061. https://doi.org/10.1016/j.compositesb.2007.11.004.
Provis, J.L., Palomo, A., Shi, C., 2015. Advances in understanding alkali-activated materials. Cement Concr. Res. 78, 110–125. https://doi.org/10.1016/j.cemconres.2015.04.013.
Ranjbar, N., Zhang, M., 2020. Fiber-reinforced geopolymer composites: a review. Cem. Concr. Compos. 107, 103498 https://doi.org/10.1016/j.cemconcomp.2019.103498.
Raoof, S.M., Koutas, L.N., Bournas, D.A., 2016. Bond between textile-reinforced mortar (TRM) and concrete substrates: experimental investigation. Compos. B Eng. 98, 350–361. https://doi.org/10.1016/j.compositesb.2016.05.041.
Redon, C., Li, V.C., Wu, C., Hoshiro, H., Saito, T., Ogawa, A., 2001. Measuring and modifying interface properties of PVA fibers in ECC matrix. J. Mater. Civ. Eng. 13, 399–406. https://doi.org/10.1061/(ASCE)0899-1561(2001)13:6(399).
Sharma, M., Gao, S., Mäder, E., Sharma, H., Wei, L.Y., Bijwe, J., 2014. Carbon fiber surfaces and composite interphases. Compos. Sci. Technol. 102, 35–50. https://doi.org/10.1016/j.compscitech.2014.07.005.
Shi, C., Qu, B., Provis, J.L., 2019. Recent progress in low-carbon binders. Cement Concr. Res. 122, 227–250. https://doi.org/10.1016/j.cemconres.2019.05.009.
Singh, S., Shukla, A., Brown, R., 2004. Pullout behavior of polypropylene fibers from cementitious matrix. Cement Concr. Res. 34, 1919–1925. https://doi.org/10.1016/j.cemconres.2004.02.014.
Tang, L., Liu, W., Zhang, Q., Dong, Z., Zhu, J., 2020. A Preparation Method and Applications of Carbon Fiber Composite. Chinese Patent No. ZL 2020 1 0456183.3. China National Intellectual Property Administration.
Tamon, H., Kitamura, T., Okazaki, M., 1998. Preparation of silica aerogel from TEOS. J. Colloid Interface Sci. 197, 353–359. https://doi.org/10.1006/jcis.1997.5269.
Trejbal, J., Kopecký, L., Tesárek, P., Fládr, J., Antoš, J., Somr, M., Nežerka, V., 2016. Impact of surface plasma treatment on the performance of PET fiber reinforcement in cementitious composites. Cement Concr. Res. 89, 276–287. https://doi.org/10.1016/j.cemconres.2016.08.018.
Vilaplana, J.L., Baeza, F.J., Galao, O., Alcocel, E.G., Zornoza, E., Garcés, P., 2016. Mechanical properties of alkali activated blast furnace slag pastes reinforced with carbon fibers. Construct. Build. Mater. 116, 63–71. https://doi.org/10.1016/j.conbuildmat.2016.04.066.
Wang, G.J., Liu, Y.W., Guo, Y.J., Zhang, Z.X., Xu, M.X., Yang, Z.X., 2007. Surface modification and characterizations of basalt fibers with non-thermal plasma. Surf. Coat. Technol. 201, 6565–6568. https://doi.org/10.1016/j.surfcoat.2006.09.069.
Wu, Z., Khayat, K.H., Shi, C., 2018. How do fiber shape and matrix composition affect fiber pullout behavior and flexural properties of UHPC? Cem. Concr. Compos. 90, 193–201. https://doi.org/10.1016/j.cemconcomp.2018.03.021.
Yurt, Ü., 2020. An experimental study on fracture energy of alkali activated slag composites incorporated different fibers. J. Build. Eng. 32, 101519 https://doi.org/10.1016/j.jobe.2020.101519.
Zhou, X., Zheng, W., Zeng, Y., Xu, C., Chen, P., 2022. Effect of fiber content and stress–strength ratio on the creep of basalt fiber–reinforced alkali-activated slag concrete. Struct. Concr. 23, 382–394. https://doi.org/10.1002/suco.202100443.
Zielke, U., Hüttinger, K.J., Hoffman, W.P., 1996. Surface-oxidized carbon fibers: I. Surface structure and chemistry. Carbon 34, 983–998. https://doi.org/10.1016/0008-6223(96)00032-2.